



Fermi National Accelerator Laboratory

FERMILAB-Pub-82/30-THY/EXP  
2000.000  
(Submitted to Z. Phys.)

THE QCD COMPTON PROCESS UP TO TEVATRON ENERGIES

A. Ng

Department of Physics and Ames Laboratory-DOE  
Iowa State University, Ames, Iowa 50011

and

R. Orava and K. E. Lassila

Fermi National Accelerator Laboratory, Batavia, Illinois 60510

April 1982

The QCD Compton Process up to Tevatron Energies  
A. Ng  
Department of Physics and Ames Laboratory-DOE  
Iowa State University,  
Ames, Iowa 50011

and

R. Orava and K.E. Lassila\*  
Fermi National Accelerator Laboratory  
Batavia, Illinois 60510

We investigate the QCD Compton effect  $\gamma q \rightarrow gq$  by using Monte Carlo methods to simulate complete three jet events for photon-nucleon interactions. This process provides unique possibilities for jet studies because the incoming photon transfers its entire energy to the final state gluon and quark jets. We present a number of predictions for photons in the range of energies presently available up to Tevatron energies and find that the QCD Compton effect will dominate over vector meson dominance at large gluon transverse momenta.

## I. Introduction

Recent studies of large transverse momentum phenomena based on Quantum Chromodynamics (QCD), have been mainly directed at the gluon bremsstrahlung processes in deeply inelastic lepton-nucleon scattering or in  $e^+e^-$  annihilation to quark-gluon jet systems [1]. A cleaner test of perturbative QCD should be possible with the QCD Compton effect,  $\gamma q \rightarrow gq$ , where the incoming real photon transfers its entire energy to the final state quark and gluon jets at high transverse momenta [2]. The point-like component of the photon entering this reaction has characteristics distinct from the hadron-like component, especially at the edges of available phase space, i.e., at high transverse momenta, high fractional parton momenta, etc., where the typical vector-meson component of the photon is sharply cut off. The particular advantage of the QCD Compton effect over gluon bremsstrahlung derives from kinematics. In the QCD Compton effect, as viewed from the photon-quark center of mass frame, there is nothing going forward in the initial photon direction to mask the produced high transverse momentum parton jets. The spectator diquark jet is relatively soft and travels in the backward c.m. direction. There are other potentially interesting hard scattering processes that have the same kinematical advantage, for example, the inverse QCD Compton effect  $qg \rightarrow q\gamma$  (direct photon

production) or photon-gluon fusion  $\gamma g \rightarrow \bar{q}q$ . In this analysis we shall concentrate on the QCD Compton effect and simulate complete events resulting from the hadronization of the final state quarks and gluons  $\gamma N \rightarrow (q\text{-jet}) + (g\text{-jet}) + (di\text{-quark - jet})$ .

## II. Event Simulation

The invariant jet cross section for the QCD Compton effect [2] as depicted in Fig. 1a is

$$E \frac{d\sigma}{d^3p} (\gamma P \rightarrow \text{jet} + X) = \frac{1}{\pi} \sum_i x_i f_i(x_i, Q^2) \frac{2}{2 - x_T e^Y} \frac{d\sigma_i}{d\hat{t}}, \quad (1)$$

where  $E$  is the c.m. energy,  $p$  the momentum of the detected particle, and  $f_i(x_i, Q^2)$  gives the momentum density distribution of quark  $i$  with momentum fraction  $x_i$  inside the proton. The differential cross section for the QCD Compton subprocess with variables as labelled in Fig. 1b is

$$\frac{d\sigma_i}{d\hat{t}} (\gamma q_i \rightarrow g q_i) = \frac{-8\pi e_i^2 \alpha \alpha_s(Q^2)}{3s} \left( \frac{\hat{u}}{\hat{s}} + \frac{\hat{s}}{\hat{u}} \right), \quad (2)$$

with  $e_i$  = fractional electric charge carried by quark  $i$ ,  $Y$  is the gluon c.m. rapidity,  $\alpha = 1/137$ , and

$$x_i = \frac{x_T e^{-Y}}{2 - x_T e^{-Y}} \quad , \quad x_T = \frac{2P_T}{\sqrt{s}} \quad ,$$

$$\alpha_s(Q^2) = 12\pi / \left[ (33 - 2N_f) \ln(Q^2/\Lambda^2) \right] ,$$

$$Q^2 = 2\hat{s} \hat{t} \hat{u} / (\hat{s}^2 + \hat{t}^2 + \hat{u}^2) \quad ,$$

$$s = (P_\gamma + P_i)^2, \quad \hat{t} = (P_\gamma - P_g)^2, \quad \hat{u} = (P_i - P_g)^2,$$

where  $\Lambda = 0.30$  GeV and we adopt Feynman's [3] definition of  $Q^2$ .

Our Monte Carlo [4] simulates complete QCD Compton events in photon-nucleon interactions in the photon-nucleon center-of-mass frame. We neglect the effective parton masses and initial parton Fermi motion inside the nucleon. We also impose restrictions on the kinematical range of variables  $Q^2$  and the momentum fraction  $x_i$  of the proton carried by parton  $i$ ,  $Q^2 > 1 \text{ GeV}^2/c^2$ ,  $0.04 \leq x_i \leq 0.99$ . For the  $Q^2$  dependent fractional momentum distributions of quarks in the target nucleon we use the Buras and Gaemers parametrization [5].

Without much loss in physical significance of our Monte Carlo simulation results, we may assume that the valence diquark system in the proton, which is the spectator to the hard photon-quark scattering, is a valence antiquark (i.e.,  $\bar{3}$ ). It moves backwards, opposite to the direction of the incoming photon beam, whereas the two large  $P_T$  jets (quark and gluon jets) move apart from each other at angles large compared to the initial photon direction.

The photon-nucleon reactions we examine produce three color systems moving separately in the center-of-mass frame of reference. We employ the standard prescription of Field and Feynman [6] to simulate the subsequent fragmentation of the color systems resulting from the confinement mechanism. We treat the radiated gluon as a quark-antiquark pair of definite flavor. The original quark of this pair carrying some fraction of the gluon momentum moves along the fragmentation axis and generates a color field in which new quark-antiquark pairs evolve. The original quark then fragments into a "leading" meson (which is not necessarily the fastest meson in the "string") by combination with an antiquark from a newly created  $q\bar{q}$  pair in the color field. The original quark transfers a portion of its momentum to the remaining quark of this new  $q\bar{q}$  pair, which then cascades further in the same manner until all the available energy and momentum are exhausted. The last "primary" meson is a

combination of a new quark and the "spectator" antiquark (di-quark). With a similar procedure a second string of primary mesons is created in such a way that the first meson has the antiquark of the gluon and the last meson contains the final state quark of the QCD Compton process  $\gamma q + gq$ .

The momenta of the new quarks (antiquarks) transverse to the fragmentation axis are distributed according to a Gaussian,  $d\sigma/dP_T^2 \propto \exp(-P_T^2/2\sigma_q^2)$ , where  $\sigma_q = 350$  MeV/c. The longitudinal momenta are distributed according to the scaling forms of the fragmentation functions proposed by Field and Feynman [6].

We utilize a recent measurement of the relative probability for generating strange quark-antiquark pairs,  $P_s$ , in the color field as compared to  $u\bar{u}(d\bar{d})$  quark pairs,  $P_s/P_u(P_s/P_d)$ , and take the probabilities to be  $P_u = P_d = 0.44$ ,  $P_s = 0.12$ , where we have neglected charmed particle production ( $P_u + P_d + P_s = 1$ ) [7].

Since the experimental data for the production ratio between primary mesons in different spin states are not accurate enough, we assume that vector and pseudoscalar mesons are produced with equal probability. This is not inconsistent with the experimental results [8].

Finally, the three-jet final states, fully simulated by our Monte Carlo program, are Lorentz transformed into the laboratory system along the z-direction which is defined by the incoming photon. Because we neglected the parton masses and transverse motion in the nucleon this transformation is satisfactory though only approximately correct.

### III. Simulation Results

We have generated 3000 QCD Compton events with different kinematical selections for each c.m. energy studied. In the following we shall study the invariant jet cross sections and general characteristics of these events.

The cross section for the reaction  $\gamma p \rightarrow \text{gluon jet} + X$  is estimated to be between 10 and 20 nb with the gluon jet at  $90^\circ$  in the overall center-of-mass frame. Figure 2 shows the theoretical prediction of the gluon jet cross section at the gluon c.m. rapidity  $Y=0$ , which falls smoothly with the gluon transverse momentum  $P_T$ . Dependence on the incident photon energy is shown in Fig. 3, where we plot the invariant cross sections for  $\sqrt{s}$  of 9.7, 15.6, 19.4 and 27.4 GeV. A  $P_T^{-4}$  behaviour is seen at  $\sqrt{s}=19.4$  GeV. The curve labelled "VMD" shows the "hadron-like" behavior of the photon as described by the vector Meson Dominance model which leads to a steeply falling cross section as a function of  $P_T$  [9]. The rapidity

distributions at different fixed  $P_T$  values are shown in Fig. 4. Concentration of produced hadrons in the jet is clearly seen at positive rapidities for each  $P_T$ .

The fragmenting quark should be dominantly a u-quark because of the electromagnetic coupling, and thus one would expect that the positively charged mesons would reflect the original quark flavor. In Fig. 5, we show the  $P_T$ -distribution,  $d\sigma/dP_T$ , for all the charged particles excluding  $\pi^+$  mesons and for  $\pi^+$  mesons only. No significant differences are observed, as expected. Note that to make absolute normalization possible we have restrictions,  $0 < Y < 1$ ,  $2 < P_T < 6.5$  GeV/c, on the final state gluon.

The expected increase in the ratio of  $\pi^+$  to  $\pi^-$  mesons in the forward hemisphere as a function of Feynman x-values and the hadron transverse momenta relative to the photon direction can be seen in Fig. 6.

The average charged multiplicity has been reported to have an energy dependence much stronger than  $\ln s$  in various experiments, such as  $e^+e^-$  annihilations and  $p\bar{p}$  collisions [10]. Our Monte Carlo generated QCD Compton events exhibit the same behavior for the average multiplicity of final state hadrons as a function of  $\sqrt{s}$ , illustrated in Fig. 7. Our prediction for the absolute charged multiplicity is much

less than the naively expected value. This will be discussed in the next section.

We show the energy dependence of the invariant mass distribution in Figs 8(a) and (b). The total invariant mass in the forward c.m. hemisphere increases faster with energy than the corresponding mass in the backward hemisphere. Characteristics of the gluon jet can also be studied by means of the energy flow outside an angular cone about the gluon jet axis in the overall center-of-mass frame. Our prediction for the energy flow [11], as shown in Fig. 9, rises sharply at small angles and shows little change as the size of the angular cone increases. This rate of energy flow also depends on the incoming photon energy, as illustrated.

#### IV. Discussions and conclusions

We have generated complete QCD Compton events where the final state production of 3 jets is studied in detail. Subsets of this analysis can be compared with the work of other authors who examine one jet. Such invariant jet cross sections, as for the  $\gamma N \rightarrow (\text{jet}) + X$  reactions, have been studied theoretically by Owens [9] and other authors [12]. Our simulation results for the invariant gluon jet cross section at various energies appear to have the same behaviour

predicted by these previous authors, (see Fig. 3). As the energy increases, the invariant gluon jet cross sections become flatter allowing us to isolate the VMD contribution from the QCD Compton processes at  $P_T$  greater than 4.5 GeV/c [9]. The hadron-like component of the photon does not give any important background at such large  $P_T$  values due to the faster decrease of the parton distribution functions in the target nucleon with increasing parton fractional momentum.

The accumulation of hadrons produced in the gluon jet at c.m. rapidities  $Y > 0$  is seen in Fig. 4. Such behaviour is also seen by plotting the invariant mass distribution,  $d\sigma/dM$  vs  $M$  for the final state hadrons in both forward and backward hemisphere as shown in Fig. 8. Without experimental data, it is reasonable to assume that there is a 50% probability for finding a gluon jet and 50% probability for finding a quark jet among the isolated jets in the laboratory. From the phenomenological point of view, the gluon jet is expected to contribute more to the average multiplicity than the quark jet. Thus we should see more hadrons in the forward hemisphere, than expected for the hadron-like photon-nucleon processes. Furthermore, as the energy increases, the leading order QCD term becomes a dominant contribution in the photon production processes, which is demonstrated by the strong increase in the number of final state hadrons in the forward cms hemisphere

relative to the backward hemisphere.

There is no obvious difference between the  $P_T$ -distribution of all charged particles without including  $\pi^+$  mesons with that due to  $\pi^+$  mesons only, as shown in Fig. 5. The ratio  $R=\pi^+/\pi^-$  of  $\pi^+$  mesons to  $\pi^-$  mesons produced in the forward c.m. hemisphere increases with increasing  $x_F$  and  $P_T$ , as shown in Fig 6, an effect illustrating the dominance of u-quark jets among the produced quark jets. The relatively slow increase of R as a function of  $x_F$  or  $P_T$  can be understood in terms of our prior assumption of equal probability for formation of  $u\bar{u}$  and  $d\bar{d}$  pairs in the color field during the fragmentation process.

Final particle multiplicities are shown in Fig. 7. We do not show the average multiplicities of  $\pi^-$  mesons and  $K^-$  mesons, because they are almost identical with those of  $\pi^+$  mesons and  $K^+$  mesons, respectively. For  $\pi^0$ -multiplicities, we roughly expect the relation  $\langle n_{\pi^0} \rangle = (\langle n_{\pi^+} \rangle + \langle n_{\pi^-} \rangle) / 2$  (Isospin symmetry) to hold. The relative number of K mesons just reflects the experimental value of the ratio  $P_s/P_u$ . From Fig. 7, we conclude that there is a strong increase in the average charged and neutral multiplicities. We would like to recommend the average charged multiplicity as a convenient quantity to measure in an experiment. For pure three-jet events we have made a conservative estimate (based

on completely independent jet production) of the average charged multiplicity at  $\sqrt{s}=27.4$  GeV, which turns out to be within the range  $20 < n_{ch} > < 30$ . However, the generated QCD Compton events predict  $\langle n_{ch} \rangle = 13.77$ , which is lower than our naive estimate. This is expected in our scheme of correlated jet production.

Fig. 9 shows the characteristics of the gluon jet in the overall center of mass frame, which can be used to differentiate it from other quark jets. The slow behaviour of these curves at angles greater than  $20^\circ$  is expected from the uncertainty principle which limits the transverse momenta of hadrons fragmenting from the gluon jet. From the phenomenological results, we used the Gaussian distribution with  $\sigma=0.35$  to generate the final hadrons.

More experimental data are needed to further study our predictions. We stress that even though, in our simulation, we ignore effective parton masses, parton Fermi motion inside the nucleon and treat the diquark as an antiquark, we should get reasonably reliable results.

We believe that the study of the QCD Compton effect via Monte Carlo techniques provides a new dimension in understanding large  $P_T$  phenomena. Our work indicates that one can identify the jet by studying the  $P_T$  distributions,

mass distributions, multiplicities, and energy flow. Some information relevant to the kinematic constraints can also be obtained from the simulation method to aid the experimental set-up of the detectors for the study of  $\gamma N$  reactions. The photon-nucleon data expected from experiments possible with the Tevatron should be able to isolate signals from the  $\gamma q \rightarrow gq$  subprocess.

References

\*Permanent address: Department of Physics, Iowa State University, Ames, Iowa 50011.

1. A.J. Buras "A Tour of Perturbative QCD" Fermilab-Conf-81/69-THY, to be published in the proceedings of the International Lepton-Photon Conference, Bonn, Germany, August 24-29, 1981.
2. H. Fritzsch and P. Minkowski, Phys. Lett 69B, 316 (1977).
3. R.P. Feynman, R.D. Field and G.C. Fox Phys. Rev. D 18, 3320 (1978).
4. The present Monte Carlo program used in this analysis is revised from the original version written by R. Orava, Fermilab, 1980 (unpublished).
5. A.J. Buras and K.J.F. Gaemers, Nucl. Phys. B132, 249 (1978), as revised by A.J. Buras, private communication.
6. R. Field and R. Feynman, Nucl. Phys. B136, 1(1978). B. Andersson, G. Gustafson, T. Sjustrand, Lund Preprint LU-TP 80-1.
7. V.V. Ammosov et al., Phys. Lett. 93B, 210(1980).
8. V.V. Ammosov et al., "Vector Meson Production in Antineutrino Neutral Current Interactions" Serpukhov preprint IFVE 81-175 (1981).
9. J.F. Owens, Phys. Rev. D21, 54(1980).
10. R. Brandelik et al. Phys. Lett. 89B, 418(1980); Ch. Berger et al. ibid95B, 313(1980); K. Alpgard et al., ibid. 107B, 315(1981).
11. G. Sterman and S. Weinberg Phys. Rev. Letters 38, 1436(1977).
12. R.J. DeWitt et al., Phys. Rev. D19, 2046(1979); D20, 1751(E) (1979); I. Kang and C.H. Llewellyn Smith, Nucl. Phys. B166, 413(1980); M. Fontannez, A. Mantrach, and D. Schiff, Z. Physik C6, 241(1980).

Figure Legends

Fig. 1(a) The photon-quark collision in the center of momentum frame indicating the final state quark, gluon and diquark jets.

(b) The QCD Compton effect for photon + quark  $\rightarrow$  gluon + quark with the subprocess kinematical variables  $\hat{s}$ ,  $\hat{t}$ ,  $\hat{u}$  labelled.

Fig. 2 Theoretical prediction for the inclusive gluon transverse momentum ( $P_T$ ) distribution in  $\Upsilon N$  interactions at  $\sqrt{s}=19.4$  GeV with the gluon rapidity equal zero.

Fig. 3 Predictions of the invariant gluon-jet cross section at various energies: ..... for  $\sqrt{s}=9.7$  GeV, .-.-.- for  $\sqrt{s}=15.6$  GeV, - - - for  $\sqrt{s}=19.4$  GeV and ---- for  $\sqrt{s}=27.4$  GeV. The vector meson dominance contribution is the curve labelled by VMD.

Fig. 4 Theoretical predictions for gluon-jet rapidity distributions at the energy  $\sqrt{s}$  of 19.4 GeV and transverse momentum  $P_T$  of 1, 2 and 4 GeV/c.

Fig. 5 Predictions of the  $P_T$  distributions for the final state hadrons: (i) unshaded area for all charged particles without including  $\pi^+$  mesons and (ii) shaded area for  $\pi^+$  mesons only, at the energy  $\sqrt{s}$  of 19.4 GeV. The gluon jets are restricted to  $0 \leq Y \leq 1$  and  $2 \leq P_T \leq 6.5$  GeV/c.

Fig. 6(a) Predictions for the ratio  $\pi^+/\pi^-$  as a function of  $X_F$  in the forward c.m. hemisphere.

(b) Predictions for the ratio  $\pi^+/\pi^-$  as a function of  $P_T$  in the forward c.m. hemisphere: ..... for  $\sqrt{s}=15.6$  GeV, - - - for  $\sqrt{s}=19.4$  GeV and ----- for  $\sqrt{s}=27.4$  GeV.

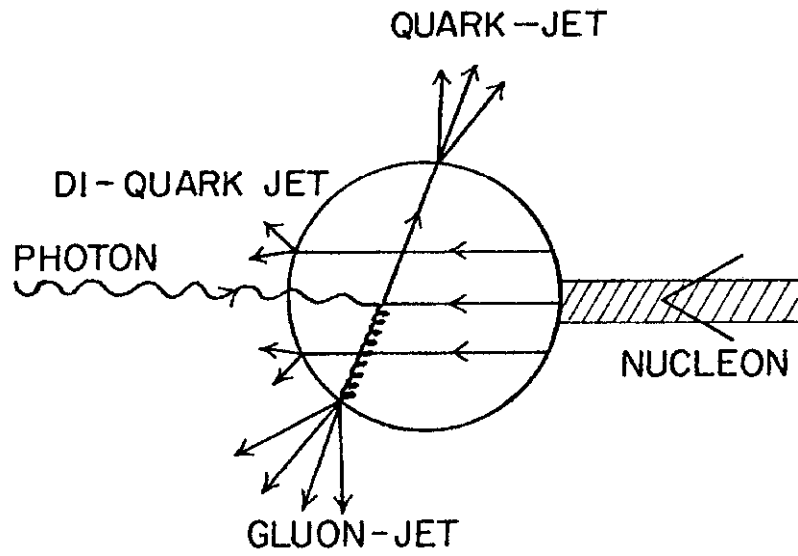
Fig. 7 Predictions for the mean multiplicities of (a)  $\pi^+$  mesons, (b)  $K^+$  mesons, (c) neutral particles and (d) all charged particles vs  $\sqrt{s}$ . Note that  $\langle \pi^- \rangle$  and  $\langle K^- \rangle$  are not shown as they are very similar to  $\langle \pi^+ \rangle$  and  $\langle K^+ \rangle$ , respectively.

Fig. 8(a) Predictions for the total invariant mass distribution for the final state hadrons in the c.m. forward and backward hemispheres: (i) unshaded area for particles with  $y > 0$  and (ii) shaded area for particles with  $y < 0$ , at

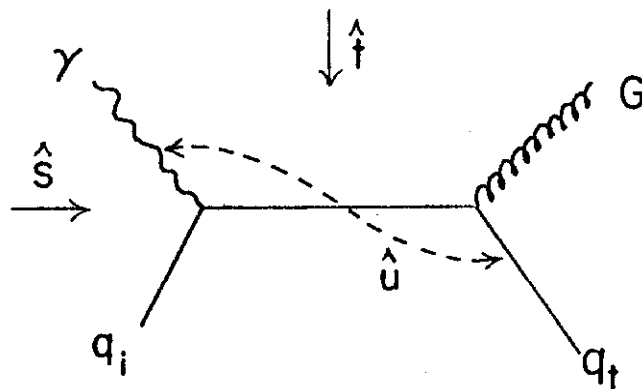
$\sqrt{s}=15.6$  GeV. The gluon jets are restricted to  $0 \leq Y \leq 1$  and  $2 \leq P_T \leq 6.5$ . Here  $M^2$  is defined as  $(\sum_{i=1} P_i)^2$  for final state hadrons.

(b) Same as (a) except  $\sqrt{s}=19.4$  GeV.

Fig. 9 Predictions for the angular energy flow outside of the cone about the gluon jet axis in the overall c.m. frame: (i) ..... for  $\sqrt{s}=9.7$  GeV, (ii) -.-.-.-. for  $\sqrt{s}=15.6$  GeV, (iii) ----- for  $\sqrt{s}=19.4$  GeV and (iv) ----- for  $\sqrt{s}=27.4$  GeV.



(a)



(b)

Figure 1

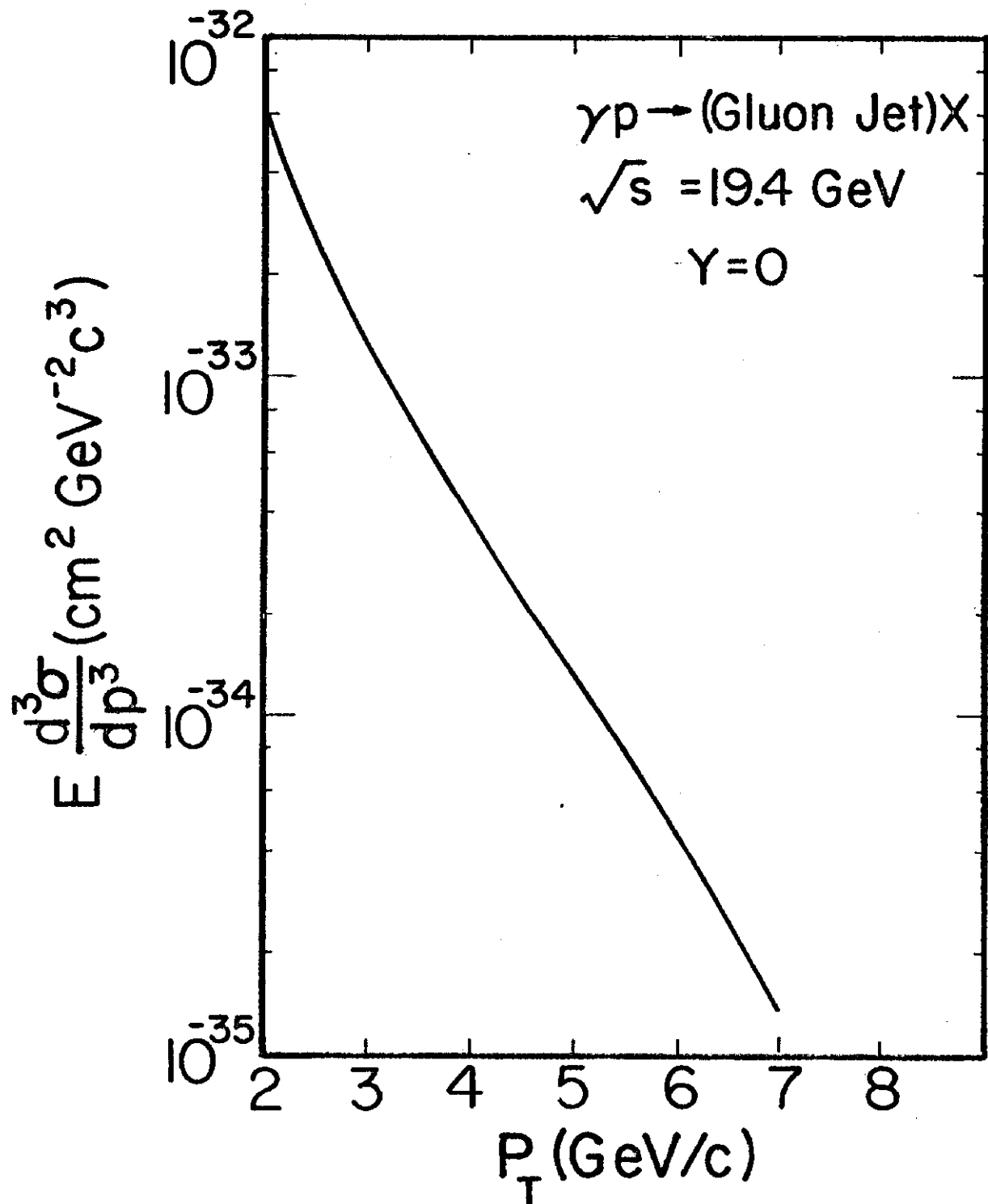


Figure 2

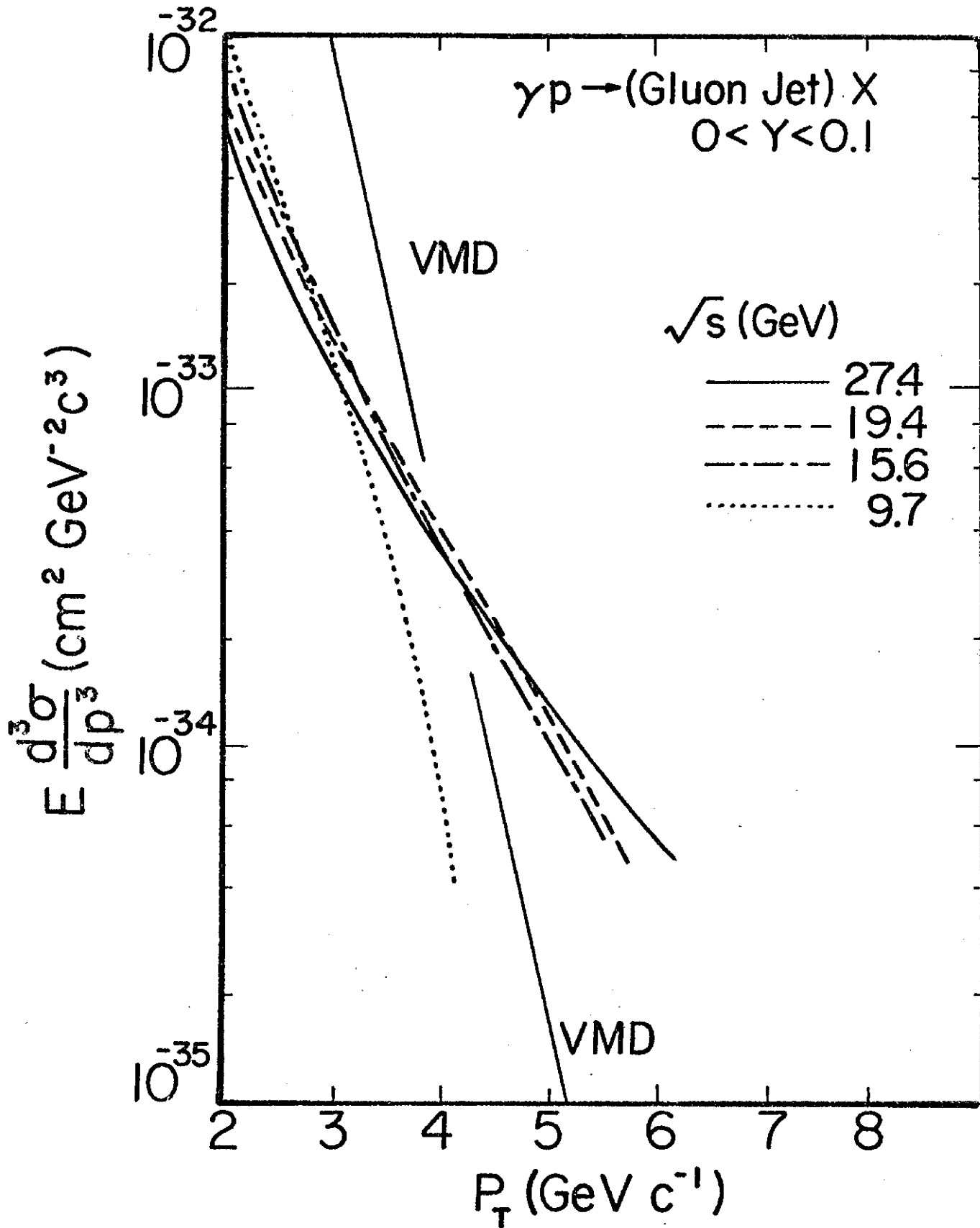


Figure 3

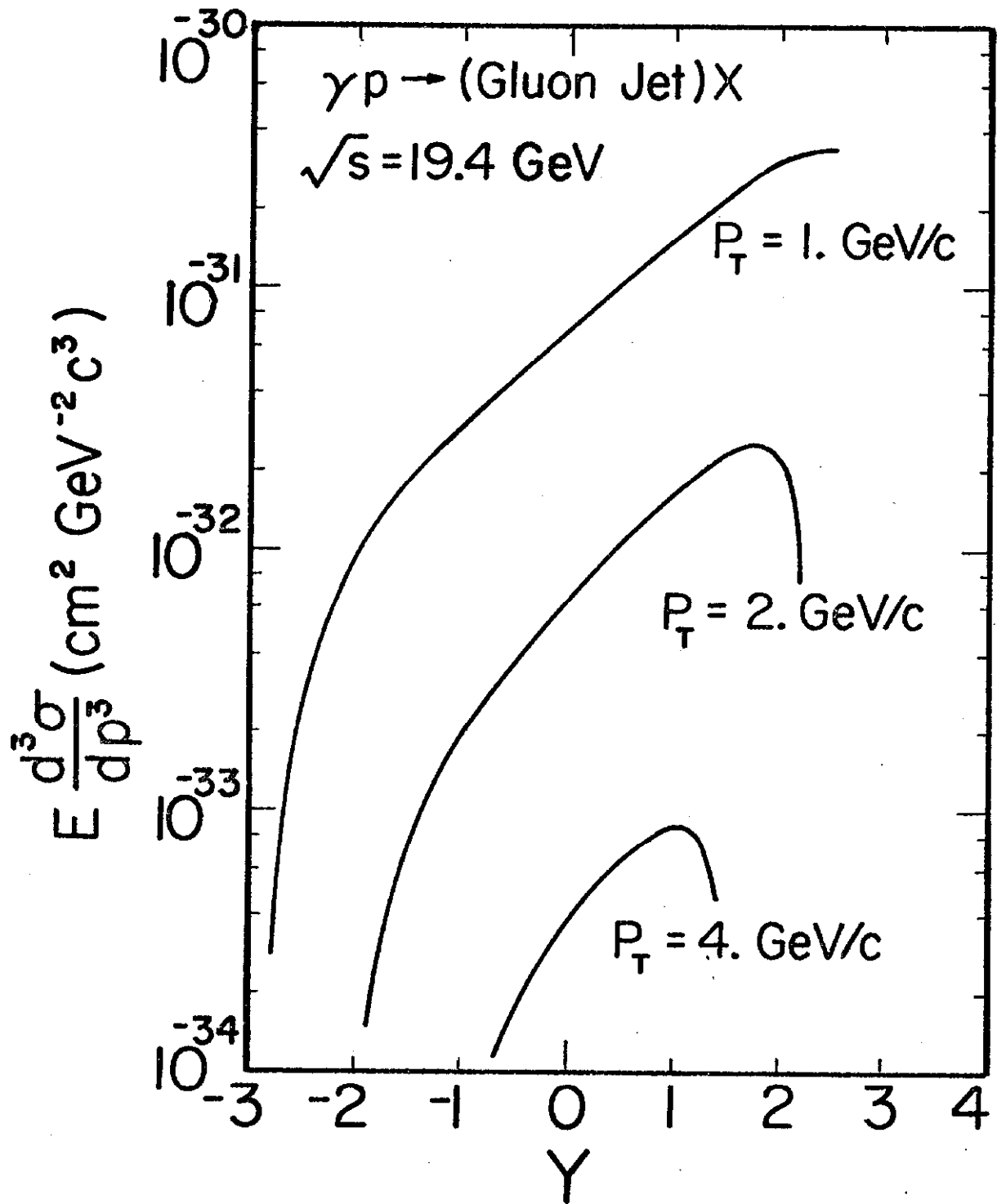


Figure 4

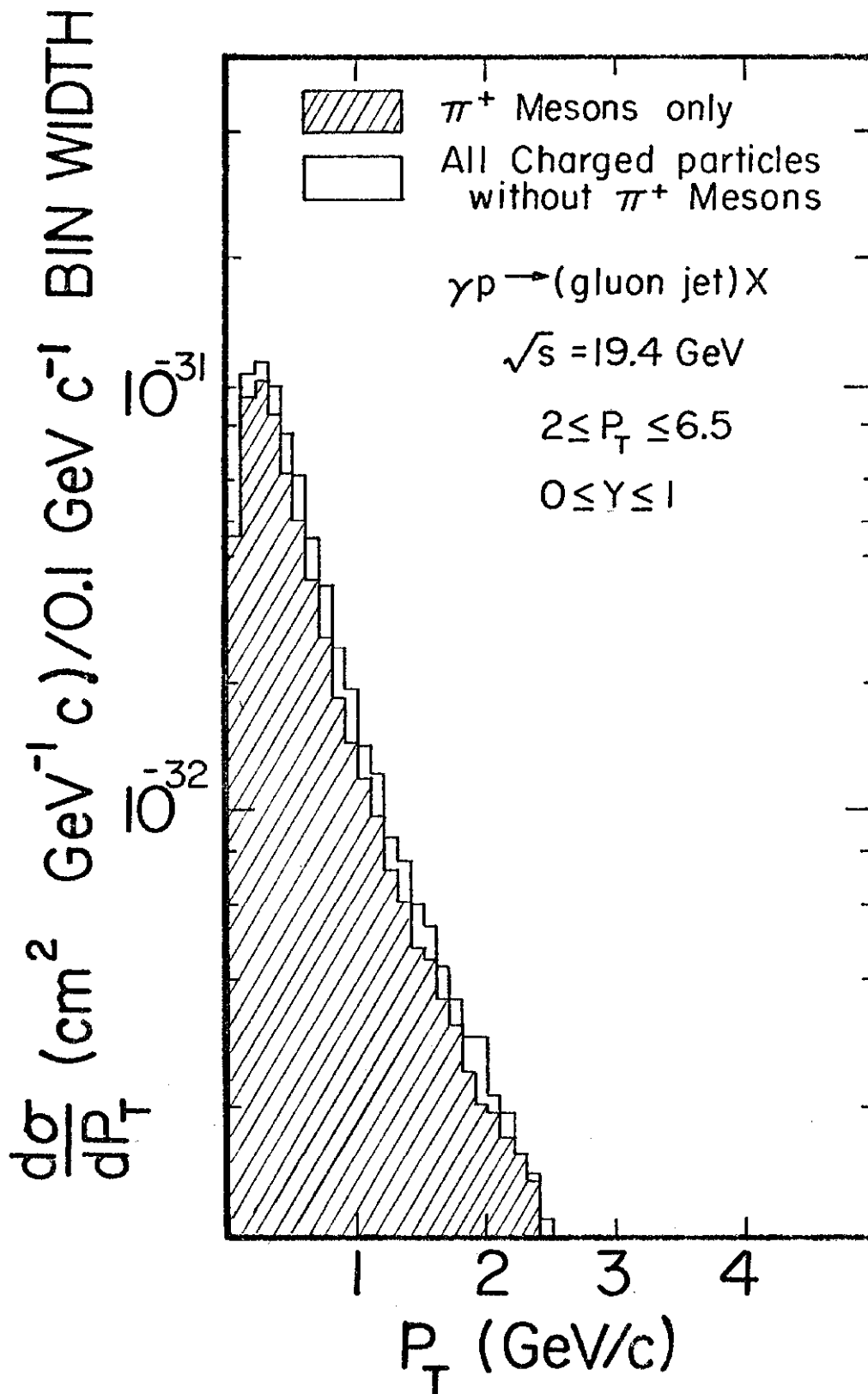


Figure 5

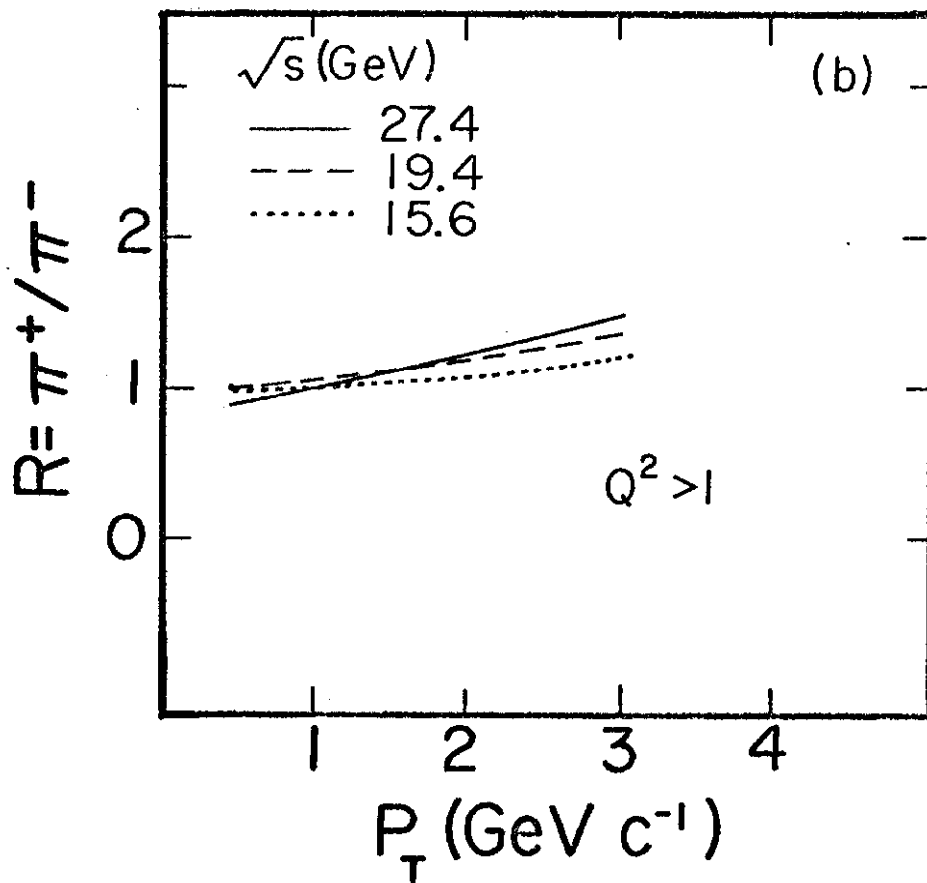
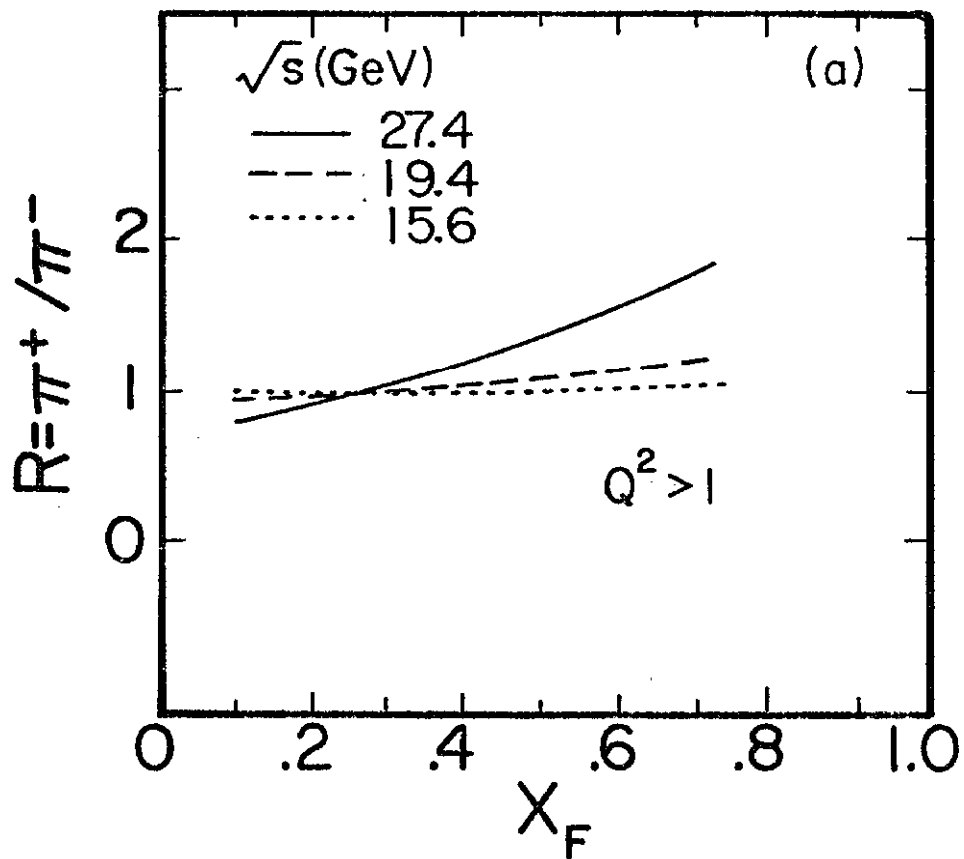


Figure 6

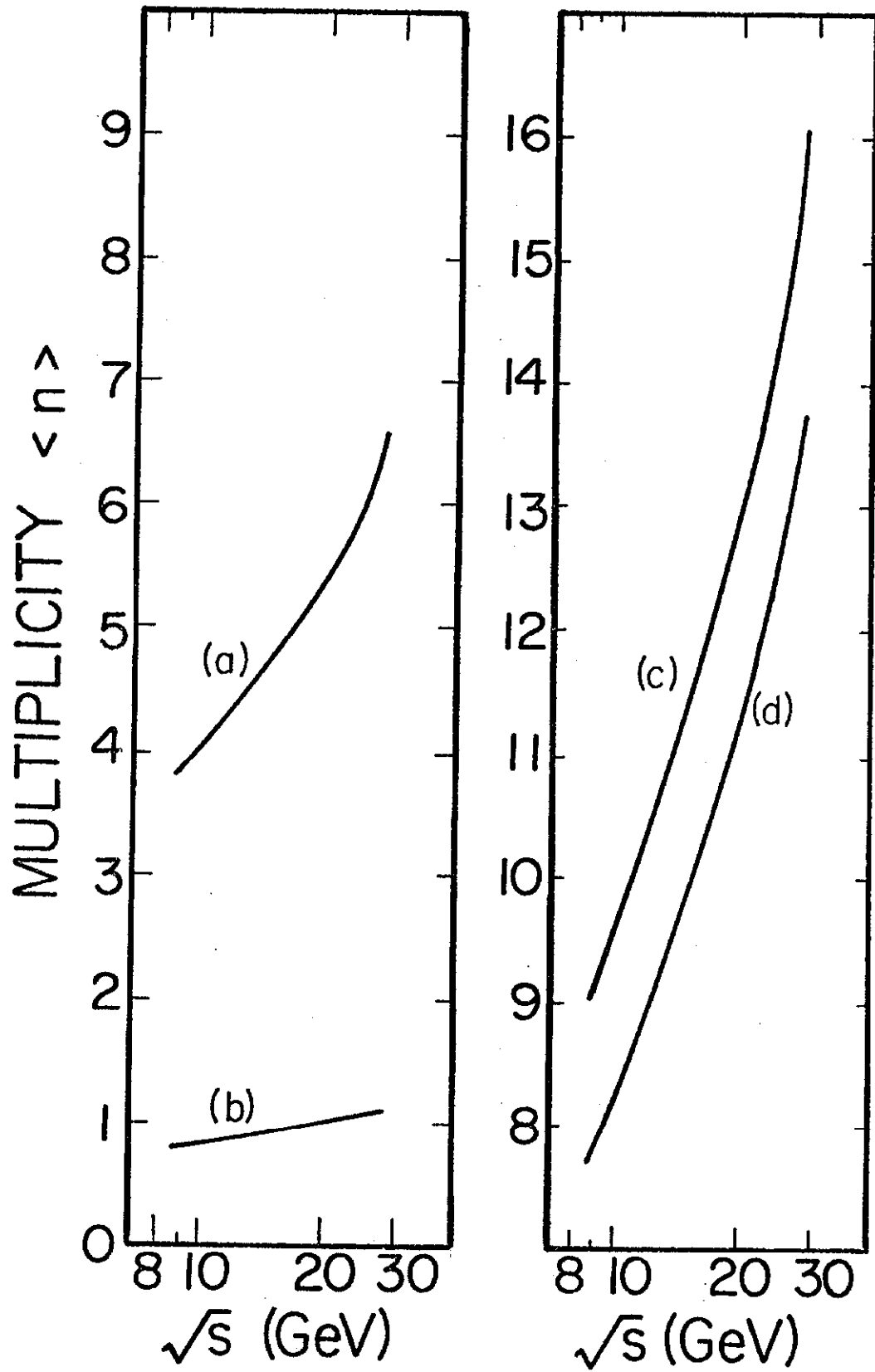


Figure 7

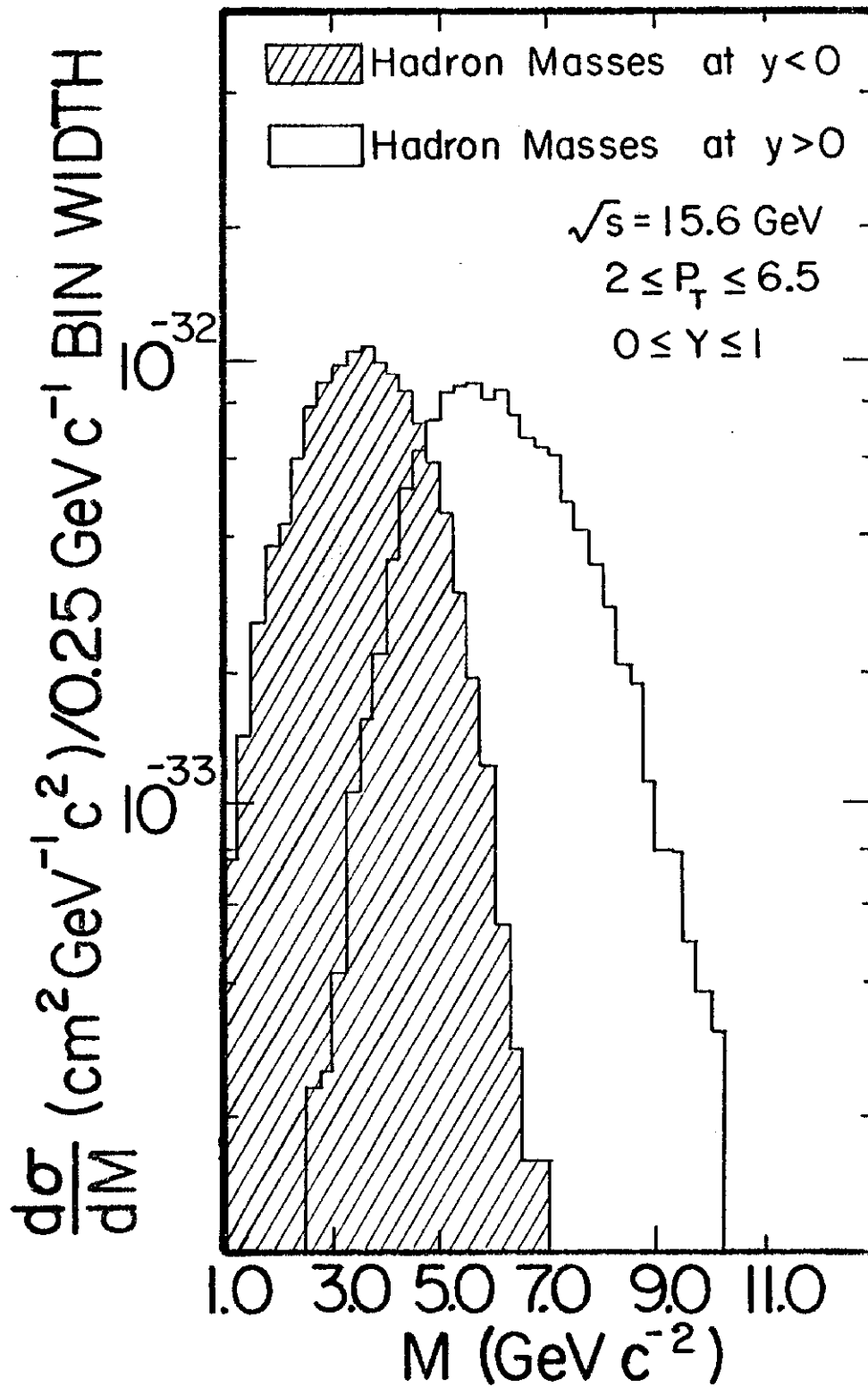


Figure 8(a)

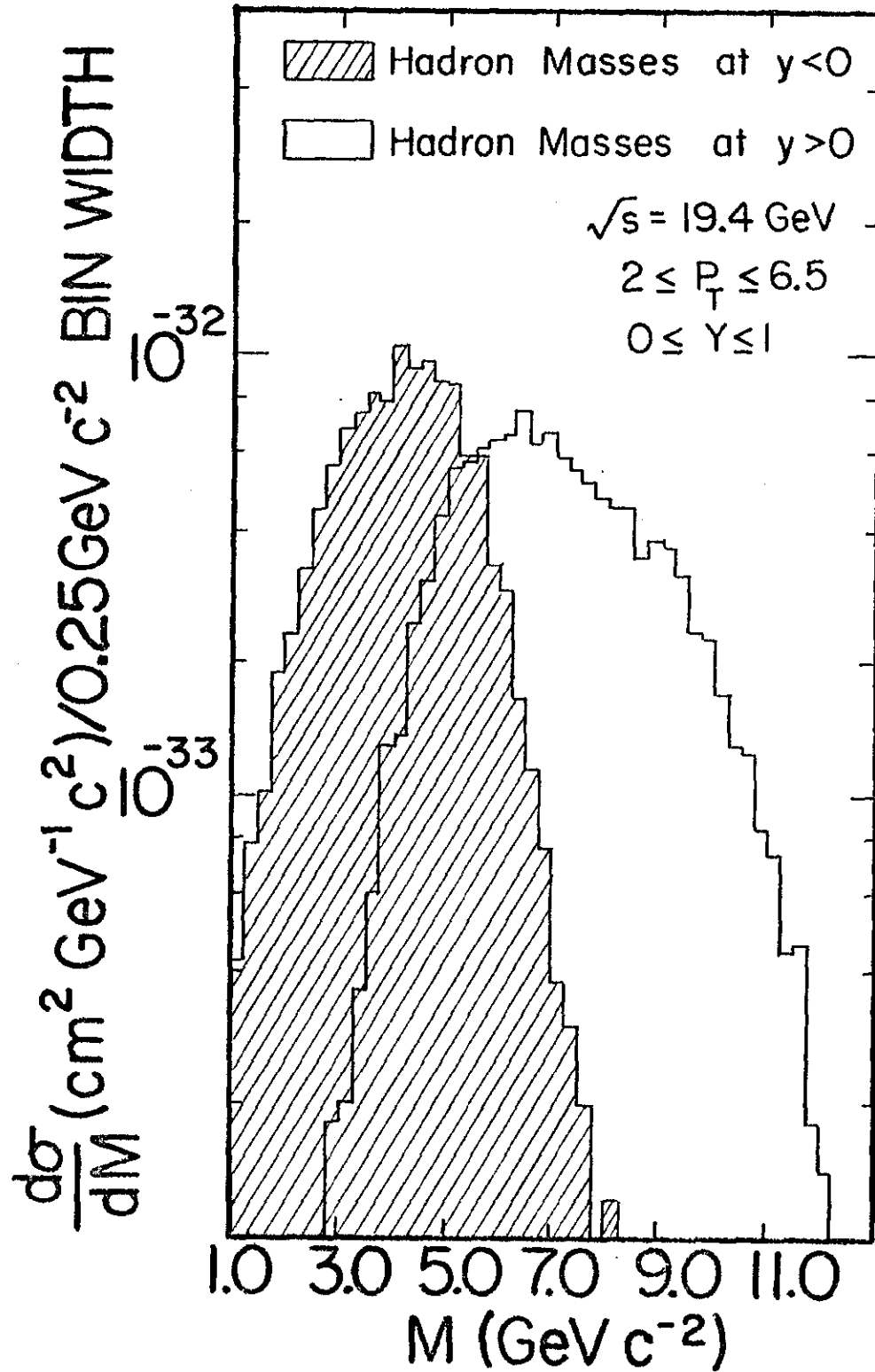


Figure 8(b)

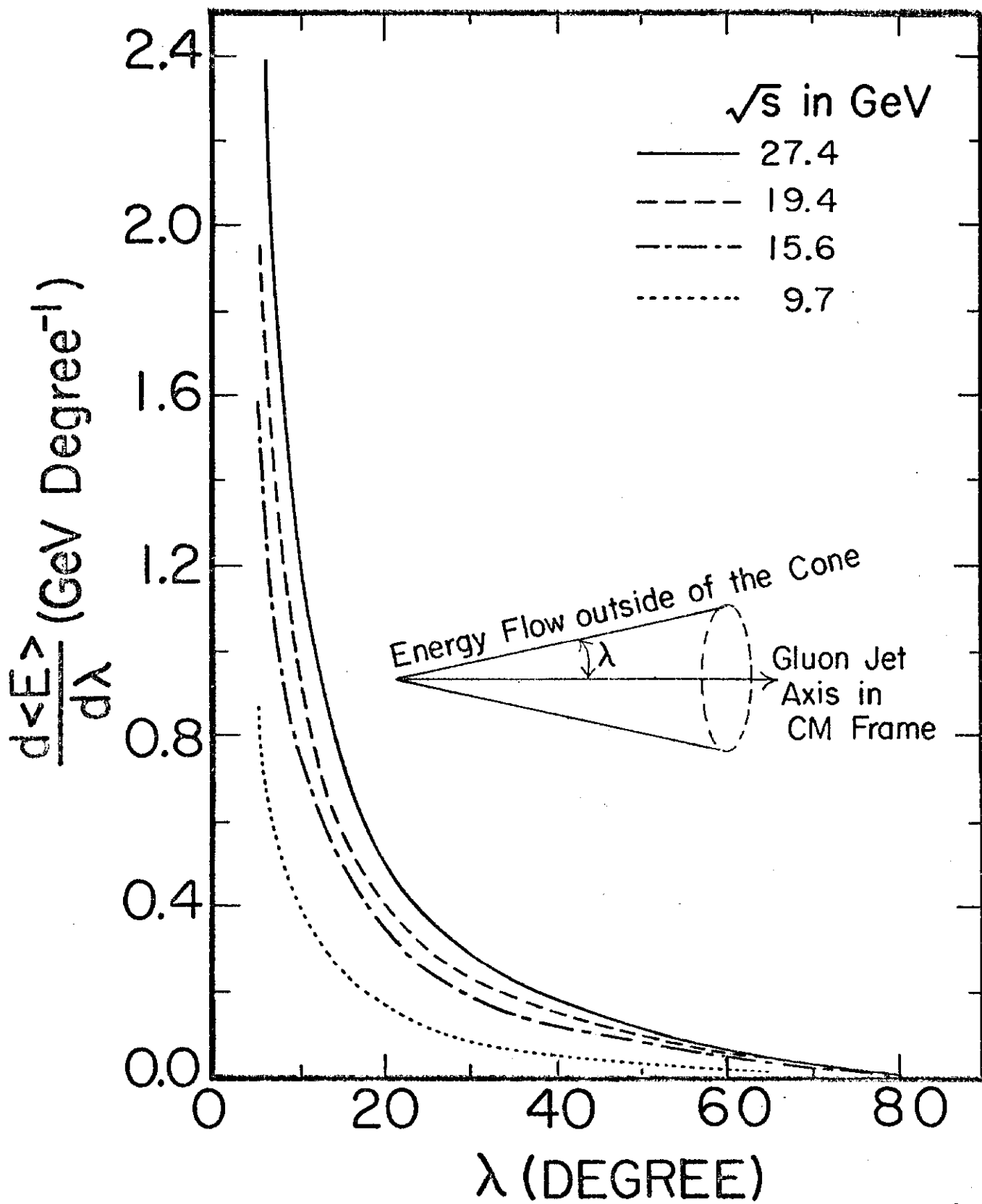


Figure 9